Extracting the mass dependence and quantum numbers of short-range correlated pairs from $A(e,e'p)$ and $A(e,e'pp)$ scattering

C. Colle,[1] O. Hen,[2] W. Cosyn,[1] I. Korover,[2] E. Piasetzky,[2] J. Ryckebusch,[1] and L. B. Weinstein[3]
[1]*Ghent University, Ghent, Belgium*
[2]*School of Physics and Astronomy, Tel Aviv University, Tel Aviv 69978, Israel*
[3]*Old Dominion University, Norfolk, Virginia, USA*
(Received 3 April 2015; published 6 August 2015)

The nuclear mass dependence of the number of short-range correlated (SRC) proton-proton (pp) and proton-neutron (pn) pairs in nuclei is a sensitive probe of the dynamics of short-range pairs in the ground state of atomic nuclei. This work presents an analysis of electroinduced single-proton and two-proton knockout measurements off ^{12}C, ^{27}Al, ^{56}Fe, and ^{208}Pb in kinematics dominated by scattering off SRC pairs. The nuclear mass dependence of the observed $A(e,e'pp)/^{12}\mathrm{C}(e,e'pp)$ cross-section ratios and the extracted number of pp- and pn-SRC pairs are much softer than the mass dependence of the total number of possible pairs. This is in agreement with a physical picture of SRC affecting predominantly nucleon-nucleon pairs in a nodeless relative-S state of the mean-field basis.

DOI: 10.1103/PhysRevC.92.024604 PACS number(s): 25.30.Rw, 25.30.Fj, 24.10.−i

I. INTRODUCTION

The nuclear momentum distribution (NMD) is often quoted as being composed of two separate parts [1–3]. Below the Fermi momentum ($k_F \approx 250$ MeV/c) single nucleons move as independent particles in a mean field created by their mutual interactions. Above the Fermi momentum ($k > k_F$) nucleons predominantly belong to short-range correlated (SRC) pairs with high relative and low center-of-mass (c.m.) momenta, where high and low are relative to the Fermi momentum [4–8]. In addition to its intrinsic interest, the NMD and its division into mean-field and correlated parts is relevant to two-component Fermi systems [9], neutrino physics [10,11], and the symmetry energy of nuclear matter [12].

The mean-field and long-range aspects of nuclear dynamics have been studied extensively since the dawn of nuclear physics. The effect of long-range correlations on the NMDs is limited to momenta which do not extend far beyond k_F [13]. Study of the short-range aspects of nuclear dynamics has blossomed with the growing availability of high-energy high-intensity electron and proton accelerators. Recent experiments confirm the predictions that SRC pairs dominate the high-momentum tails ($k > k_F$) of the NMDs [4–7], accounting for 20–25 % of the NMD probability density [14–17]. These high-momentum tails have approximately the same shape for all nuclei [2,3,9,14–18], differing only by scale factors which can be interpreted as a measure of the relative number of SRC pairs in the different nuclei. In this work, we aim at understanding the underlying dynamics which give rise to this universal behavior of the high-momentum tail.

An intuitive picture describing the dynamics of nuclei including SRCs is that of independent bound nucleons moving in the nucleus, occasionally getting sufficiently close to each other to temporarily fluctuate into SRC-induced nucleon-nucleon pairs. This picture can be formally implemented in a framework in which one shifts the complexity of the nuclear SRC from the wave functions to the operators by calculating independent-particle model (IPM) Slater determinant wave functions and acting on them with correlation operators to include the effect of SRCs [18–20]. The observed number of proton-proton (pp) and proton-neutron (pn) SRC pairs in various nuclei can then be used to constrain the amount and the quantum numbers of the initial-state IPM nucleon-nucleon (SRC-prone) pairs that can fluctuate dynamically into SRC pairs through the action of correlation operators.

In this paper, we will extract the relative number of pp-SRC and pn-SRC pairs in different nuclei from measurements of electroinduced two-proton and one-proton knockout cross-section ratios for medium and heavy nuclei (^{27}Al, ^{56}Fe, and ^{208}Pb) relative to ^{12}C in kinematics dominated by scattering off SRC pairs [8,21]. In these kinematics in the plane-wave approximation $A(e,e'pp)$ cross sections are proportional to the number of pp pairs in the nucleus and $A(e,e'p)$ cross sections are proportional to twice the number of pp pairs plus the number of pn pairs ($2pp + pn$). Therefore, after correcting the measured cross sections for rescattering of the outgoing nucleons from the residual nucleus (final state interactions or FSIs), the relative number of pp and pn pairs will be extracted from measurements of $A(e,e'pp)/^{12}\mathrm{C}(e,e'pp)$ and $A(e,e'p)/^{12}\mathrm{C}(e,e'p)$ cross-section ratios [8].

We will then compare the $A(e,e'pp)/^{12}\mathrm{C}(e,e'pp)$ cross-section ratios and the extracted number of pp and pn pairs to factorized calculations using different models of nucleon pairs in order to deduce the quantum numbers of the IPM SRC-prone pairs. We will provide strong evidence that the relative quantum numbers of the majority of the SRC-susceptible pairs are $^1S_0(1)$ for pp and $^3S_1(0)$ for pn. Hereby, we used the notation $^{2J+1}L_S(T)$ to identify the pair's quantum state (T is the total isospin).

This paper is structured as follows. The one- and two-proton knockout experiments analyzed in this paper are described in Sec. II. In Sec. III we introduce the model to calculate the FSI-corrected two-nucleon knockout cross-section ratios. Results and discussions are presented in Sec. IV. Section V contains the concluding remarks.

II. EXPERIMENT

The one- and two-proton knockout measurements analyzed in this paper were described in [8] and its supplemental information. They were carried out using the CEBAF Large Acceptance Spectrometer (CLAS) [22], located in Hall-B of the Thomas Jefferson National Accelerator Facility (Jefferson Lab) in Newport News, Virginia. The data were collected in 2004 using a 5.014 GeV electron beam incident on ^{12}C, ^{27}Al, ^{56}Fe, and ^{208}Pb targets. The scattered electron and knocked out proton(s) were measured with CLAS. We selected $A(e,e'p)$ events in which the electron interacts with a single fast proton from a SRC nucleon-nucleon pair in the nucleus by requiring large four-momentum transfer ($Q^2 > 1.5$ GeV^2), Bjorken scaling parameter $x_B = \frac{Q^2}{2m_N\omega} > 1.2$, and missing momentum $300 < |\vec{p}_{\rm miss}| < 600$ MeV/c. The four-momentum transfer $Q^2 = \vec{q}\cdot\vec{q} - (\frac{\omega}{c})^2$ where $\vec{q}$ and ω are the three-momentum and energy transferred to the nucleus respectively; m_N is the nucleon mass; the missing momentum $\vec{p}_{\rm miss} = \vec{p}_p - \vec{q}$, and $\vec{p}_p$ is the knockout proton three-momentum. We also required that the knockout proton was detected within a cone of 25° of the momentum transfer $\vec{q}$ and that it carried at least 60% of its momentum (i.e., $\frac{|\vec{p}_p|}{|\vec{q}|} \geqslant 0.6$). To suppress contributions from inelastic excitations of the struck nucleon we limited the reconstructed missing mass of the two-nucleon system $m_{\rm miss} < 1.1$ GeV/c^2.

The $A(e,e'pp)$ event sample contains all $A(e,e'p)$ events in which a second, recoil, proton was detected with momentum greater than 350 MeV/c. Figure 1 shows the distribution of the cosine of the angle between the initial momentum of the knockout proton and the recoil proton for these events [8]. The recoil proton is emitted almost diametrically opposite to the missing-momentum direction. The observed backward-peaked angular distributions are very similar for all nuclei and are not due to acceptance effects as shown by the angular distribution of mixed events. These distributions are a signature of scattering on a nucleon in a SRC pair, indicating that the two emitted protons were largely back-to-back in the initial state, having large relative momentum and small c.m. momentum [6,23]. Further evidence of scattering on a SRC nucleon pair is that the recoil proton was emitted at forward angles (i.e., angles in the range 20°–60° with respect to $\vec{q}$).

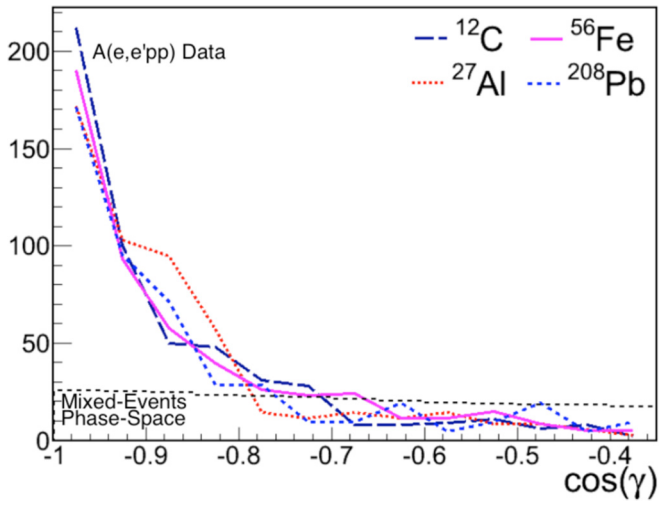

FIG. 1. (Color online) Distribution (in arbitrary units) of the cosine of the angle γ between the missing momentum of the leading proton and the recoil proton for ^{12}C (dark blue long-dashed line), ^{27}Al (red dotted line), ^{56}Fe (purple solid line), and ^{208}Pb (blue dashed line). The black dashed line shows the distribution of the random phase-space extracted from mixed events.

The $A(e,e'p)/^{12}$C$(e,e'p)$ and $A(e,e'pp)/^{12}$C$(e,e'pp)$ cross-section ratios are obtained from the ratio of the measured number of events, normalized by the incident integrated electron flux and the nuclear density of each target. During the experiment all solid targets were held in the same location, the detector instantaneous rate was kept constant, and the kinematics of the measured events from all target nuclei were almost identical [8,21]. Therefore detector acceptance effects cancel almost entirely in the $A(e,e'pp)$/C$(e,e'pp)$ cross-section ratios. Due to the large acceptance of CLAS, radiative effects affect mainly the electron kinematics. These corrections were calculated in Ref. [21] for the extraction of the $A(e,e'p)$/C$(e,e'p)$ cross-section ratio. As the electron kinematics is the same for the $A(e,e'p)$ and $A(e,e'pp)$ reactions, the same corrections are used here to extract the $A(e,e'pp)$/C$(e,e'pp)$ cross-section ratios. See Ref. [8] for additional details.

III. FSI AND CROSS-SECTION MODEL

To extract the underlying relative number of pp and pn SRC pairs in nuclei from the measured cross-section ratios, we must correct the data for FSI effects [8]. Alternatively, in order to compare the measured ratios to calculations, we must correct either the data or the calculation for FSI effects. The two dominant contributions are (1) attenuation of the outgoing nucleon(s) upon traversing the residual $A-1$ or $A-2$ nucleus, and (2) rescattering of a neutron into a proton [i.e., single charge-exchange (SCX)]. SCX can lead to a pp final state which originates from a pn pair.

The effect of FSIs of the ejected pair with the remaining $A-2$ spectators was computed in a relativistic multiple-scattering Glauber approximation (RMSGA) [24,25]. The RMSGA is a multiple-scattering formalism based on the eikonal approximation with spin-independent NN interactions. We have included both the elastic and the SCX rescattering of the outgoing nucleons with the $A-2$ spectators. The three parameters entering in the RMSGA model are taken from NN scattering data and yield an excellent description of the world's $A(e,e'p)$ transparency data [25]. In this work no free parameters are tuned to model the FSI effects in the $A(e,e'p)$ and $A(e,e'pp)$ data under study. The RMSGA yields attenuation coefficients that are similar to the power-law results obtained in nuclear transparency measurements [21]. For those reasons, we estimate the systematic uncertainty related to the FSI calculation as small.

The SCX probabilities are calculated in a semiclassical approximation. The probability of charge-exchange re-scattering for a nucleon with initial IPM quantum numbers α which is brought in a continuum state at the coordinate $\vec{r}$ is

modeled by

$$P_{\rm CX}^{\alpha(\beta)}(\vec{r}\,) = 1 - \exp\left[-\sigma_{\rm CX}(s)\int_z^{+\infty} dz' \rho^{\alpha\beta}(z')\right]. \quad (1)$$

The z axis is chosen along the direction of propagation of the nucleon with initial quantum numbers α. The quantum numbers of the correlated partner in the SRC pair are denoted with β. The $\rho^{\alpha\beta}$ is the IPM one-body density of the residual nucleus available for SCX reactions. The $\rho^{\alpha\beta}$ is determined as the IPM density of the target nucleus, minus the contribution from the single-particle orbitals α and β. Obviously, for an ejected proton (neutron) only the neutron (proton) density of the residual nucleus affects SCX reactions. $\sigma_{\rm CX}(s)$ in Eq. (1), with s the total c.m. energy squared of the two nucleons involved in the SCX [26], can be extracted from elastic proton-neutron scattering data [27].

As outlined in Refs. [23,28], in the spectator approximation it is possible to factorize the $A(e,e'pN)$ cross section in kinematics probing short-range correlated pairs as

$$\frac{d^8\sigma[A(e,e'pN)]}{d^2\Omega_{e'}\,d^3\vec{P}_{12}\,d^3\vec{k}_{12}} = K_{epN}\,\sigma_{epN}(\vec{k}_{12})F_A^{pN(D)}(\vec{P}_{12}), \quad (2)$$

where $\Omega_{e'}$ is the solid angle of the scattered electron, and $\vec{k}_{12}$ and $\vec{P}_{12}$ are the relative and c.m. momenta of the nucleon pair that absorbed the virtual photon. The K_{epN} is a kinematic factor and $\sigma_{epN}(\vec{k}_{12})$ is the cross section for virtual-photon absorption on a correlated pN pair. The $F_A^{pN(D)}(\vec{P}_{12})$ is the distorted two-body c.m. momentum distribution of the correlated pN pair. In the limit of vanishing FSIs, it is the conditional c.m. momentum distribution of a pN pair with relative $S_{n=0}$ quantum numbers. Distortions of $F_A^{pN(D)}(\vec{P}_{12})$ due to FSI are calculated in the RMSGA. The factorized cross-section expression of Eq. (2) hinges on the validity of the zero-range approximation (ZRA), which amounts to putting the relative pair coordinate $\vec{r}_{12}$ to zero. The ZRA works as a projection operator for selecting the very-short-range components of the IPM relative pair wave functions.

The probability for charge-exchange reactions in pN knockout is calculated on an event per event basis, using the SRC pair probability density $F_A^{pN(D)}(\vec{R}_{12})$ in the ZRA corrected for FSI. With the aid of the factorized cross-section expression of Eq. (2), the phase-space integrated $A(e,e'pN)$ to ^{12}C$(e,e'pN)$ cross-section ratios can be approximately expressed as integrals over distorted c.m. momentum distributions,

$$\begin{aligned}\frac{\sigma[A(e,e'pN)]}{\sigma[^{12}{\rm C}(e,e'pN)]} &\approx \frac{\int d^2\Omega_{e'}\,d^3\vec{k}_{12}K_{epN}\,\sigma_{epN}(\vec{k}_{12})\int d^3\vec{P}_{12}F_A^{pN(D)}(\vec{P}_{12})}{\int d^2\Omega_{e'}\,d^3\vec{k}_{12}K_{epN}\,\sigma_{epN}(\vec{k}_{12})\int d^3\vec{P}_{12}F_C^{pN(D)}(\vec{P}_{12})}\\ &= \frac{\int d^3\vec{P}_{12}F_A^{pN(D)}(\vec{P}_{12})}{\int d^3\vec{P}_{12}F_C^{pN(D)}(\vec{P}_{12})}. \end{aligned} \quad (3)$$

In the absence of FSI, the integrated c.m. momentum distributions $\int d^3\vec{P}_{12}F_A^{pN(D)}(\vec{P}_{12})$ equal the total number of SRC-prone pN pairs in the nucleus A. Hence, the cross-section ratios of Eq. (3) provide access to the relative number of SRC pN pairs up to corrections stemming from FSI. We have evaluated the ratios of the distorted c.m. momentum distributions of Eq. (3) over the phase space covered in the experiment. Given the almost 4π phase space and the high computational requirement of multidimensional FSI calculations, we use an importance-sampling approach. The major effect on the c.m. momentum distribution $F_A^{pN(D)}(\vec{P}_{12})$ when including FSIs is an overall attenuation; the shape is almost unaffected [23]. Motivated by this, we used the c.m. momentum distributions without FSI as the sampling distribution for the importance sampling in the FSI calculations. When convergence is reached, the computed impact of FSI is extrapolated to the whole phase space.

IV. RESULTS AND DISCUSSIONS

Figure 2 shows the measured uncorrected $\frac{\sigma[A(e,e'pp)]}{\sigma[^{12}{\rm C}(e,e'pp)]}$ cross-section ratios compared with the ZRA reaction-model calculation with and without RMSGA FSI corrections. The first striking observation is that the measured cross-section ratios increase very slowly with A (e.g., the Pb/C ratio is only 3.8 ± 0.5). For contrast, combinatorial scaling based on the number of pp pairs leads to a ratio of over 200. The ZRA-RMSGA calculations agree well with the measured data, yielding a Pb/C ratio of $4.96^{+0.11}_{-0.14}$. The ZRA and ZRA-RMSGA calculations assume that only pairs with a finite probability density at relative coordinate zero contribute to the cross section. This is consistent with assuming that only IPM pairs in a nodeless relative-S state (i.e., $S_{n=0}$) contribute.

Figure 3 shows the number of pp- and pn-SRC pairs in various nuclei relative to carbon extracted from the measured $A(e,e'pp)$/C$(e,e'pp)$ and $A(e,e'p)$/C$(e,e'p)$ cross-section ratios following the method outlined in Ref. [8] with RMSGA corrections for FSI and SCX. The extracted number of pp pairs are very sensitive to SCX. If the virtual photon is absorbed on a pn pair and the neutron subsequently undergoes a single

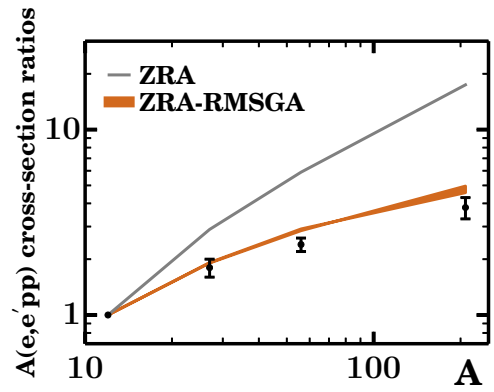

FIG. 2. (Color online) The mass dependence of the $A(e,e'pp)/^{12}$C$(e,e'pp)$ cross-section ratios. The points show the measured, FSI-uncorrected, cross-section ratios. The lower orange band and upper grey line denote ZRA reaction-model calculations for ^{12}C, ^{27}Al, ^{56}Fe, and ^{208}Pb based on Eq. (3) with and without FSI corrections respectively. The width of the ZRA-RMSGA band reflects the maximum possible effect of SCX.

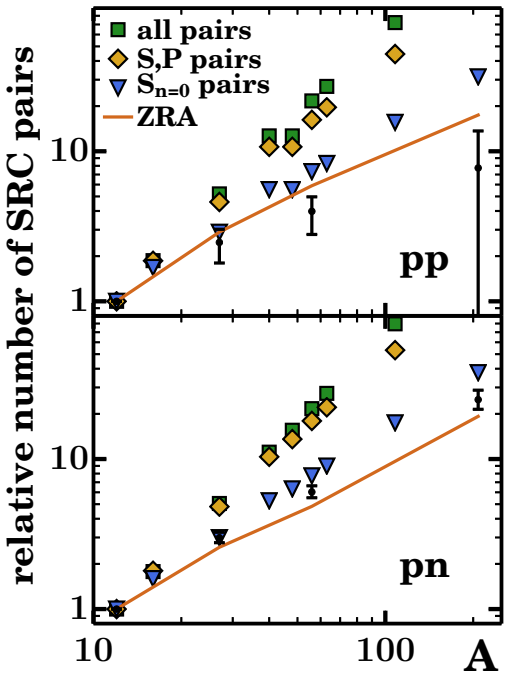

FIG. 3. (Color online) Mass dependence of the number of *pp* (top panel) and *pn* (bottom panel) SRC pairs of nucleus A relative to ^{12}C. Data (small black circles with error bars) are extracted from the measured CLAS $A(e,e'p)$ and $A(e,e'pp)$ cross-section ratios [8,21] after correcting for FSI. Error bars include the estimated uncertainty on the cross-section ratios and the FSI corrections. The green squares correspond with unconditional counting of the *pp* pairs, i.e., $[Z(Z-1)/30$ in the upper panel] and *pn* pairs ($ZN/36$ in the bottom panel) for the nuclei ^{12}C, ^{16}O, ^{27}Al, ^{40}Ca, ^{48}Ca, ^{56}Fe, ^{63}Cu, ^{108}Ag, and ^{208}Pb. The yellow diamonds are the ratios obtained by counting IPM pairs in a relative S and P state. The blue triangles count IPM $S_{n=0}$ pairs. The solid line denotes the result of a reaction-model calculation for scattering from close-proximity pairs [Eq. (3)] which takes full account of the experimental phase space. This calculation does not include FSI corrections because these are applied to the data, see text for details.

charge-exchange reaction with a proton, two protons will be detected in the final state. These events must be subtracted in order to extract the number of *pp*-SRC pairs. Since the contribution from these *pn* pairs to the *pp* final state is comparable to the number of initial *pp* pairs, this leads to a large uncertainty in the number of *pp* pairs, especially for heavy nuclei.

Figure 3 also shows the expected number of *pp* and *pn* SRC pairs relative to carbon for different quantum numbers of the IPM pairs that can dynamically form SRC pairs through the action of correlation operators. These include (a) all possible *NN* pairs (i.e., $Z(Z-1)/(6\times5)$ and $ZN/(6\times6)$ for *pp* and *pn* pairs respectively), (b) pairs in a nodeless relative-S state (i.e., $S_{n=0}$), and (c) $L\leqslant1$ pairs (i.e., both S and P state pairs). Those $S_{n=0}$ pairs are characterized by the $(n=0,L=0)$ quantum numbers for their relative orbital motion. Of all possible states for the pairs, the $S_{n=0}$ pairs have the highest probability for the two nucleons in the pair to approach each other closely. Close-proximity IPM *pn* pairs in a $^3S_1(0)$ state

TABLE I. Relative number of SRC *pp* and *pn* pairs calculated using $S_{n=0}$ counting and the ZRA reaction model compared to the extracted values from the measured $A(e,e'p)$ and $A(e,e'pp)$ ratios after correcting for FSI effects. The error includes the uncertainties in the cross-section ratios and FSI calculations.

	pp			*pn*		
	$S_{n=0}$	ZRA	Expt.	$S_{n=0}$	ZRA	Expt.
^{27}Al / ^{12}C	3.10	2.89	$2.47^{+0.55}_{-0.67}$	2.99	2.52	$2.99^{+0.26}_{-0.22}$
^{56}Fe / ^{12}C	8.60	5.89	$3.98^{+0.99}_{-1.19}$	7.72	4.82	$6.03^{+0.60}_{-0.51}$
^{208}Pb / ^{12}C	45.29	17.44	$7.73^{+5.92}_{-7.23}$	37.62	18.80	$24.87^{+3.89}_{-3.42}$

are highly susceptible to the tensor correlation operator that creates SRC pairs in a spin-triplet state with predominantly deuteron-like quantum numbers $(L=0,2;T=0;S=1)$.

We determine the number of pairs in each case using an IPM harmonic-oscillator basis and performing a standard transformation to relative and center-of-mass coordinates as detailed in Ref. [29]. The relative number of pairs are displayed in Fig. 3 and listed in Table I. As can be seen, both (a) the naive combinatorial assumption and (c) the calculations that include IPM S and P pair contributions both drastically overestimate the increase in the number of pairs with A. The ZRA and $S_{n=0}$ pair counting calculations are in fair agreement with the extracted number of *pp* and *pn* pairs.

As both the ZRA and the $S_{n=0}$ pair counting methods project IPM states onto close-range pairs, we expect the two methods to produce a similar mass dependence of the number of SRC pairs. The ZRA predicts a somewhat softer mass dependence ($\propto A^{1.01\pm0.02}$ vs $A^{1.12\pm0.02}$). This can be explained by the fact that the ZRA is a more restrictive projection on close-proximity pairs than the $S_{n=0}$ counting which accounts also for $\vec{r}_{12}\neq0$ contributions.

The observed agreement with the experimental data indicates that correlation operators acting on IPM $S_{n=0}$ pairs are responsible for the largest fraction of the high-momentum nucleons in nuclei. This gives further support to the assumption that the number of IPM pairs with quantum numbers $S_{n=0}$ is a good proxy for the number of correlated pairs in any nucleus A [18,29,30]. This is also consistent with an analysis of the cross section of the ground-state to ground-state transition in high-resolution ^{16}O$(e,e'pp)^{14}$C measurements [31,32] which provided evidence for the $^1S_0(1)$ dominance in SRC-prone *pp* pairs.

V. CONCLUSIONS

We have extracted the relative number of *pn* and *pp* SRC correlated pairs in nucleus A relative to carbon from previously published measured $A(e,e'pp)/\mathrm{C}(e,e'pp)$ and $A(e,e'p)/\mathrm{C}(e,e'p)$ cross-section ratios corrected for final state interactions. The relative number of *pn* and *pp* pairs increases much more slowly with A than expected from simple combinatorics.

We calculated the cross section in a framework which shifts the complexity of the nuclear SRC from the wave functions to the operators by calculating independent-particle model (IPM)

Slater determinant wave functions and acting on them with correlation operators to include the effect of SRCs [18–20]. The uncorrected $A(e,e'pp)/C(e,e'pp)$ cross-section ratios are consistent with a zero range approximation (ZRA) calculation that includes the effects of FSI.

Due to factorization, the ratio of calculated cross sections is approximately equal to the ratio of the distorted c.m. momentum distributions. In the absence of FSI, the integrated c.m. momentum distribution equals the total number of SRC-prone pairs in that nucleus. We compared three choices of SRC-prone pairs to the data: (a) all pairs, (b) pairs in a nodeless relative-S state ($S_{n=0}$), and (c) $L \leqslant 1$ pairs (i.e., both S and P).

We found that the soft mass dependence of the measured $A(e,e'pp)$ cross-section ratios agrees with scattering from highly selective close-proximity pairs (i.e., only IPM relative $S_{n=0}$ pairs). The mass dependence of the extracted ratios of the number of short-range correlated pp and pn pairs provides additional support for this conclusion. All these results consistently hint at a physical picture whereby the aggregated effect of SRC in the nuclear wave function is determined to a large extent by mass-independent correlation operators on $S_{n=0}$ pairs. This provides additional evidence for the scale separation between the mean-field and SRC dynamics that has, for example, been used in calculations of NMD of Refs. [18–20]. Among other things, these conclusions are likely to affect the models used to estimate the effect of correlated pairs on neutrino-nucleus cross sections [33] and studies of the nuclear equation-of-state in conditions of increased density, i.e., enhanced sensitivity of SRC [34].

ACKNOWLEDGMENTS

We acknowledge the efforts of the Jefferson Lab staff that made this experiment possible and the EG2 group and CLAS Collaboration. The Ghent group is supported by the Research Foundation Flanders (FWO-Flanders) and by the Interuniversity Attraction Poles Programme P7/12 initiated by the Belgian Science Policy Office. For the theoretical calculations, the computational resources (Stevin Supercomputer Infrastructure) and services used in this work were provided by Ghent University, the Hercules Foundation, and the Flemish Government. O. Hen and E. Piasetzky are supported by the Israeli Science Foundation. L. B. Weinstein is supported by the US Department of Energy under Grants No. de-SC00006801 and No. DOE-FG02-96ER40960.

[1] O. Benhar, A. Fabrocini, S. Fantoni, and I. Sick, Nucl. Phys. A **579**, 493 (1994).
[2] M. Alvioli, C. Ciofi degli Atti, L. P. Kaptari, C. B. Mezzetti, and H. Morita, Phys. Rev. C **87**, 034603 (2013).
[3] R. B. Wiringa, R. Schiavilla, S. C. Pieper, and J. Carlson, Phys. Rev. C **89**, 024305 (2014).
[4] A. Tang, J. W. Watson, J. Aclander, J. Alster, G. Asryan, Y. Averichev, D. Barton, V. Baturin, N. Bukhtoyarova, A. Carroll *et al.*, Phys. Rev. Lett. **90**, 042301 (2003).
[5] E. Piasetzky, M. Sargsian, L. Frankfurt, M. Strikman, and J. W. Watson, Phys. Rev. Lett. **97**, 162504 (2006).
[6] R. Subedi, R. Shneor, P. Monaghan, B. Anderson, K. Aniol, J. Annand, J. Arrington, H. Benaoum, F. Benmokhtar, W. Boeglin *et al.*, Science **320**, 1476 (2008).
[7] I. Korover, N. Muangma, O. Hen, R. Shneor, V. Sulkosky, A. Kelleher, S. Gilad, D. W. Higinbotham, E. Piasetzky, J. W. Watson *et al.* (Jefferson Lab Hall A Collaboration), Phys. Rev. Lett. **113**, 022501 (2014).
[8] O. Hen, M. Sargsian, L. B. Weinstein, E. Piasetzky, H. Hakobyan, D. W. Higinbotham, M. Braverman, W. K. Brooks, S. Gilad, K. P. Adhikari *et al.*, Science **346**, 614 (2014).
[9] O. Hen, L. Weinstein, E. Piasetzky, G. A. Miller, M. M. Sargsian, and Y. Sagi, arXiv:1407.8175.
[10] L. Fields *et al.*, Phys. Rev. Lett. **111**, 022501 (2013).
[11] G. A. Fiorentini *et al.*, Phys. Rev. Lett. **111**, 022502 (2013).
[12] O. Hen, B.-A. Li, W.-J. Guo, L. B. Weinstein, and E. Piasetzky, Phys. Rev. C **91**, 025803 (2015).
[13] W. Dickhoff and C. Barbieri, Prog. Part. Nucl. Phys. **52**, 377 (2004).
[14] L. L. Frankfurt, M. I. Strikman, D. B. Day, and M. Sargsyan, Phys. Rev. C **48**, 2451 (1993).
[15] K. S. Egiyan, N. Dashyan, M. Sargsian, S. Stepanyan, L. B. Weinstein, G. Adams, P. Ambrozewicz, E. Anciant, M. Anghinolfi, B. Asavapibhop *et al.* (CLAS Collaboration), Phys. Rev. C **68**, 014313 (2003).
[16] K. S. Egiyan, N. B. Dashyan, M. M. Sargsian, M. I. Strikman, L. B. Weinstein, G. Adams, P. Ambrozewicz, M. Anghinolfi, B. Asavapibhop, G. Asryan *et al.* (CLAS Collaboration), Phys. Rev. Lett. **96**, 082501 (2006).
[17] N. Fomin, J. Arrington, R. Asaturyan, F. Benmokhtar, W. Boeglin, P. Bosted, A. Bruell, M. H. S. Bukhari, M. E. Christy, E. Chudakov *et al.*, Phys. Rev. Lett. **108**, 092502 (2012).
[18] J. Ryckebusch, M. Vanhalst, and W. Cosyn, J. Phys. G **42**, 055104 (2015).
[19] R. Roth, T. Neff, and H. Feldmeier, Prog. Part. Nucl. Phys. **65**, 50 (2010).
[20] S. K. Bogner and D. Roscher, Phys. Rev. C **86**, 064304 (2012).
[21] O. Hen *et al.* (CLAS Collaboration), Phys. Lett. B **722**, 63 (2013).
[22] B. Mecking *et al.* (CLAS Collaboration), Nucl. Instrum. Methods Phys. Res., Sect. A **503**, 513 (2003).
[23] C. Colle, W. Cosyn, J. Ryckebusch, and M. Vanhalst, Phys. Rev. C **89**, 024603 (2014).
[24] J. Ryckebusch, D. Debruyne, P. Lava, S. Janssen, B. Van Overmeire, and T. Van Cauteren, Nucl. Phys. A **728**, 226 (2003).
[25] W. Cosyn and J. Ryckebusch, Phys. Rev. C **87**, 064608 (2013).
[26] W. R. Gibbs and B. Loiseau, Phys. Rev. C **50**, 2742 (1994).
[27] M. Jain, M. L. Evans, G. Glass, J. C. Hiebert, R. A. Kenefick, L. C. Northcliffe, B. E. Bonner, J. E. Simmons, C. W. Bjork, P. J. Riley *et al.*, Phys. Rev. C **30**, 566 (1984).
[28] J. Ryckebusch, Phys. Lett. B **383**, 1 (1996).
[29] M. Vanhalst, W. Cosyn, and J. Ryckebusch, Phys. Rev. C **84**, 031302 (2011).
[30] M. Vanhalst, J. Ryckebusch, and W. Cosyn, Phys. Rev. C **86**, 044619 (2012).

[31] C. J. G. Onderwater *et al.*, Phys. Rev. Lett. **78**, 4893 (1997).

[32] R. Starink, M. van Batenburg, E. Cisbani, W. Dickhoff, S. Frullani, F. Garibaldi, C. Giusti, D. Groep, P. Heimberg, W. Hesselink *et al.*, Phys. Lett. B **474**, 33 (2000).

[33] R. Acciarri, C. Adams, J. Asaadi, B. Baller, T. Bolton, C. Bromberg, F. Cavanna, E. Church, D. Edmunds, A. Ereditato *et al.*, Phys. Rev. D **90**, 012008 (2014).

[34] Xin Zhang, Chang Xu, Zhongzhou Ren, Eur. Phys. J. A **50**, 113 (2014).